RSC Advances

ROYAL SOCIETY OF CHEMISTRY

www.rsc.org/advances

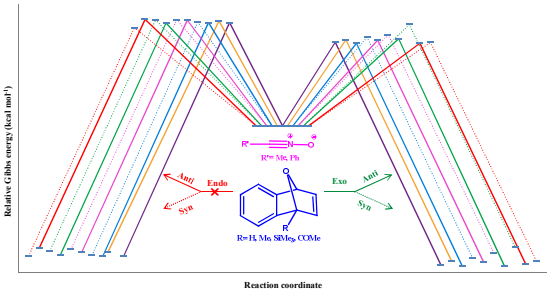

The origin of *exo/anti* selectivity in the 1,3-dipolar cycloaddition of nitrile oxides with C1-substituted 7-oxabenzonorbornadienes have been investigated theoretically.

The origin of regio- and stereoselectivity in 1,3-dipolar cycloaddition of nitrile oxides with C_1-substituted 7-oxabenzonorbornadienes, A DFT study

M. Bakavoli, M. Gholizadeh, H. Eshghi, M. Izadyar and J. Tajabadi*

In this computational study, density functional theory (DFT) calculations were performed in order to achieve a deep understanding of the regio- and stereoselectivity of 1,3-dipolar cycloadditions (1,3-DC) of C_1-substituted 7-oxabenzonorbornadienes (OBNDs) **(2a-2d)** with acetonitrile oxide **(1a)** and benzonitrile oxide **(1b)**. The potential energy surface analysis, Wiberg bond orders (BOs) and global electron density transfer (GEDT) at the transition states (TSs) show that these cycloadditions take place through a low asynchronous one-step mechanism with none polar character. Mechanism studies display these reactions are *exo*-stereoselective and *anti*-regioselective **(3X)** and classified as (*pseudodiradical*) *pr-type* 1,3-DC reactions. These results are in excellent agreement with the experimental observations. Distortion-interaction model has been used successfully for understanding of regio- and stereoselectivity in these reactions.

Keywords: regioselectivity, stereoselectivity, 1,3-dipolar cycloaddition, 7-oxabenzonorbornadienes, nitrile oxides, distortion-interaction model.

1. Introduction

2-Isoxazolines (4,5-dihydroisoxazoles)[1] are the building blocks of numerous fused heterocyclic compounds exhibiting various biological activities, such as antimicrobial and antifungal,[2] anti-inflammatory,[3] herbicide and insecticide[4] as well as anticancer activity.[5] The reductive cleavage of N-O bond in the isoxazoline ring can lead to stereoselective construction of many synthetically important compounds, such as β-hydroxy ketones, 1,3-amino alcohols, or 1,3-diols.[6] A paramount synthetic strategy for one step synthesis of isoxazolines is the cycloaddition of alkenes with nitrile oxides.[7] Bicyclic and hetero bicyclic alkenes serve as valuable precursors for the creation of highly substituted cyclic and acyclic systems because of their unusual geometry and high reactivity.[8]

In the past decades, the understanding of the underlying principles in cycloaddition reactions has grown from a fruitful interplay between theory and experiment and continues to present a real challenge. One of frequently studied phenomena in the 1,3-dipolar cycloaddition (1,3-DC) reactions with activated double bond of strained bicyclic systems is their remarkable stereoselectivity and indeed, with norbornene and norbornadiene derivatives proceeds on the *exo* face (with respect to the methylene bridge).[9] In the 1,3-DC reactions of oxabicyclo [2,2,1] heptadiene systems also, *exo*-rule prevails.[10] Moreover, unsymmetrically substituted norbornenes and norbornadienes have been reported to undergo cycloaddition reactions with complete stereoselectively.[11] The desired *exo*-isomers are the one in which oxygen of the dipole is attached to the more substituted center of the dipolarophiles. It should be noted the violation of the *exo*-rule in 1,3-DC reactions of bicycle [2.2.1] alkenes has been observed in some cases.[12] Recently, William Tam *et al*. reported the synthesis of novel oxabicycle fused isoxazolines *via* 1,3-DC reactions of acetonitrile oxide (**1a**) and benzonitrile oxide (**1b**) with unsymmetrical C_1-substituted 7-oxabenzonorbornadienes (OBNDs) (**2a-2d**).[13] They concluded that the formed isoxazolines show complete *exo*-stereoselectivity and major preference for positioning of the nitrile oxide R' moiety *anti* to the C_1-substituent, resulting from the different atomic charge densities at C_2 and C_3 atoms of OBNDs (Scheme 1).

A literature survey revealed that there is no report on any theoretical calculations concerning the origin of regio- and stereoselectivity of 1,3-DC reactions of OBNDs with nitrile oxides. Intrigued by these findings and due to our interest in applying the theoretical methods to study of the 1,3-DC reactions,[14] a theoretical study on the above reactions was performed, in order to achieve a deeper insight to regio- and stereoselectivity of these 1,3-DC reactions. In this paper, potential energy surface analysis, conceptual density functional theory (DFT) indices and distortion/interaction model are applied and we wish to report our findings pertaining the origin of regio- and stereoselectivity of OBNDs with nitrile oxides using DFT/B3LYP/6-31G(d) calculations.

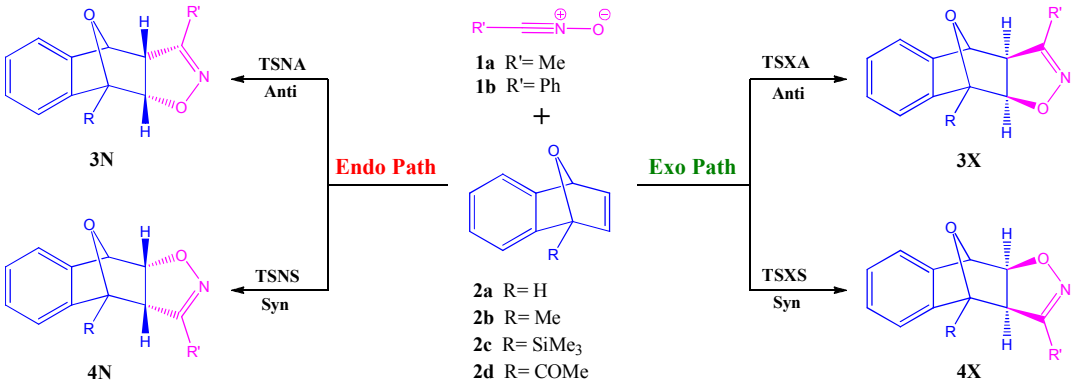

Scheme 1. Stereo- and regioisomeric channels associated with the 1,3-DC reactions of OBNDs **2a-2d** with nitrile oxides **1a-1b**.

2. Computational details

All computations were carried out with the Gaussian 09 program suite.[15] Geometry optimization of all stationary points was carried out using DFT methods at the B3LYP/6-31G(d) level of theory.[16] This economical method predicts barriers within a mean absolute deviation of 1.5 kcal mol^{-1} compared to CBS-QB3.[17] Simon and Goodman suggested geometry optimization and frequency calculation by hybrid GGA functionals, (*e.g.* B3LYP), followed by a single-point calculation using a hybrid meta-GGA functional (*e.g.* M05-2X), which gives reasonably good results compared with transition states (TSs) which optimized with more expensive hybrid meta-GGA functionals.[18] Therefore, we carried out a single-point calculation using M05-2X(UF)/6-311++G(2d,2p) (integral = grid = ultrafine) on the B3LYP/6-31G(d) geometries.

In all calculations, the ideal gas approximation, at the standard conditions was assumed. Reactants and products were characterized by frequency computations and have positive definite Hessian matrices. The TSs had only one negative eigenvalue in their diagonalized force constant matrices. The vibrational mode was assigned appropriately by means of visual inspection and animation using the GaussView 5 program.[19] The intrinsic reaction coordinate (IRC) calculations were performed on the TSs to determine the connectivity of the TS structure to the corresponding product and reactant using the second-order González–Schlegel integration method.[20] The population of regioisomers was calculated by taking into account the Gibbs energies using the Boltzmann distribution under the experimental conditions. Variational and tunneling effects were neglected in these calculations.

The distortion/interaction model developed by Ess and Houk provides a highly insightful method for understanding reactivity and activation barriers in cycloadditions.[21] Decomposition of the activation energy ($\Delta E^{\ddagger}$) for bimolecular reactions into the distortion energy ($\Delta E_d^{\ddagger}$) and the energy of interaction ($\Delta E_i^{\ddagger}$) between distorted fragments, yields valuable insight into the difference between the activation energies of the *endo* and *exo* pathways. The distortion energy ($\Delta E_d^{\ddagger}$) is the energy required to geometric and electronic change to deform the reactants into the geometries they possess at the TSs without allowing interaction between the addends. This involves bond stretching, angle decrease or increase, dihedral changes, rehybridization, etc. The interaction energy is comprised of repulsive exchange-repulsions (Pauli repulsions) and stabilizing electrostatic, polarization, and orbital (covalent) effects on the TS structure. The activation barrier is the sum of these two terms, according to eq. 1

$$\Delta E^{\ddagger} = \Delta E_d^{\ddagger} + \Delta E_i^{\ddagger} \qquad \text{(eq. 1)}$$

where *E* can be electronic, enthalpic or Gibbs energy.

Natural bond orbital (NBO) analysis was performed on the electronic structures of the stationary points according to Reed *et al.*[22]

The conceptual DFT indices[23] are used as a powerful tool to predict the chemical reactivity. The electron transfer process can be characterized by the electrophilicity index proposed by Parr *et al.*,[24] which measures the capacity of the molecule to undergo partial electron transfer. The global electrophilicity index is given by the following simple formula: $\omega = \mu^2/2\eta$. This index is expressed in terms of the electronic chemical potential μ and the chemical hardness η. Both quantities may be obtained in terms of the electron energies of the frontier molecular orbital, highest occupied molecular orbital (HOMO) and lowest unoccupied molecular orbital (LUMO), ε_H *and* ε_L, *as* $\mu = (\varepsilon_H + \varepsilon_L)/2$ *and* $\eta = (\varepsilon_L - \varepsilon_H)$, respectively.[25] The empirical (relative) nucleophilicity index, N, has been introduced by Domingo.[26] It is based on the HOMO energies of nucleophile (Nu) and tetracyanoethylene (TCE), taken as a reference and defined as $N = \varepsilon\text{H(Nu)} - \varepsilon\text{H(TCE)}$.

3. Results and discussion

The obtained results are divided into three parts. In the first part, an analysis of the DFT reactivity indices at the ground state of the reagents is given. In the second part, we have elaborated on the energetic and structural aspects of the TSs. Finally, an account on the origin of regio- and stereoselectivity of reactions of unsymmetrical OBNDs with nitrile oxides are given.

3.1. Analysis of the DFT reactivity indices of reactants

The global DFT reactivity indices of the reactants are provided in Table S1. The electronic chemical potentials of acetonitrile oxide **(1a)** and benzonitrile oxide **(1b)** are slightly higher and lower than that of the OBND dipolarophiles, respectively. This low difference between the electronic chemical potential of dipole/dipolarophile pairs (0.28-0.66 eV) indicates that in these reactions, the electron flux along the cycloadditions[27] is very low, hence, these 1,3-DC reactions have a non-polar character. According to the absolute scale of electrophilicity[28] and nucleophilicity[29] based on ω and N index, acetonitrile oxide **(1a)** and benzonitrile oxide **(1b)** can be classified as marginal and moderate electrophiles with ω indices of 0.55 (**1a**) and 1.46 (**1b**) eV respectively . However, both compounds with moderate nucleophilic N indices, 2.39 (**1a**) and 2.78 (**1b**) eV, are classified as moderate nucleophiles. On the other hand, OBNDs can be classified as moderate electrophiles and strong nucleophiles. The inclusion of electron withdrawing group (COMe) on the C_1 carbon of OBND, lowers the HOMO and LUMO energy levels, therefore, increases the electrophilicity and decreases nucleophilicity indices, slightly. Electron releasing groups (Me and $SiMe_3$) show different behavior. Electrophilicity difference of dipole/dipolarophile pair is a useful tool to describe the electronic pattern expected for the TS structures in 1,3-DC reactions, describing non-polar ($\Delta\omega$ small) or polar ($\Delta\omega$ big) mechanisms.[30] Since this index is small for studied reactions (0.38-0.53 eV), the reactions of **1a** and **1b** nitrile oxides with **2a-2d** OBNDs are non-polar, in agreement with the electronic chemical potentials.

Finally, the non-polar character of these 1,3-DC reactions was evaluated by computing the global electron density transfer (GEDT) at the corresponding TSs. The natural atomic charges at the TSs, obtained through the NBO analysis, are shared between the nitrile oxides and the oxabicyclic frameworks. The GEDT values at the TSs are shown in Table 1. Negligible GEDT values (0.00-0.02 e) at all TSs indicate that these reactions are non-polar because of the low electrophilic character of OBNDs.

A useful classification of 1,3-DC reactions into *pseudodiradical-type* (*pr-type*) and *zwitterionic-type* (*zw-type*) reactions has been proposed.[31] *pr-type* reactions take place easily through an earlier TS with non-polar character, and *zw-type* reactions, taking place through polar TSs. It can be concluded our investigated reactions participate in *pr-type* reactions.

Recently, Domingo proposed the new local reactivity, Parr functions, in polar organic reactions.[32] In the present study, OBNDs are not electrophilically activated, hence, these 1,3-DC reactions are non-polar. Therefore, Parr functions cannot give information about the regioselectivity in these non-polar 1,3-DC reactions. He claimed that the Fukui functions based on finite charge differentiations lead to some severe errors, because the electrophilic/nucleophilic behavior of these reactions are not correspond to changes in charge distribution, as proposed by these Fukui functions. So, the Fukui functions also could not be used for prediction of regioselectivity in these non-polar reactions.

3.2. Analysis of the energetic and structural aspects of the TSs

The stationary points on the 1,3-DC reactions of acetonitrile oxide (**1a**) and benzonitrile oxide (**1b**) with unsymmetrical C_1-substituted **OBNDs** (**2a-2d**) are shown in Scheme 1. The potential energy diagram (PED), corresponding to these reactions is illustrated in Figure 1. For each of these cycloadditions, the nitrile oxide dipole could theoretically approach from either the *exo* face or the *endo* face of the bicyclic substrates. As a result, two stereoisomeric outcomes for the cycloadducts (CAs) could be envisioned. Moreover, except for symmetric **OBND** (**2a**), all its singly substituted **OBNDs** react with dipoles on two different regioisomeric pathways. Therefore, in theory, four distinct types of CAs could arise due to the possibility of the nitrile oxide R' group orienting *anti* (**3**) or *syn* (**4**) to the C1-substituent of the **OBNDs**, in addition to the five-membered ring situating stereochemically *exo* (**X**) or *endo* (**N**).

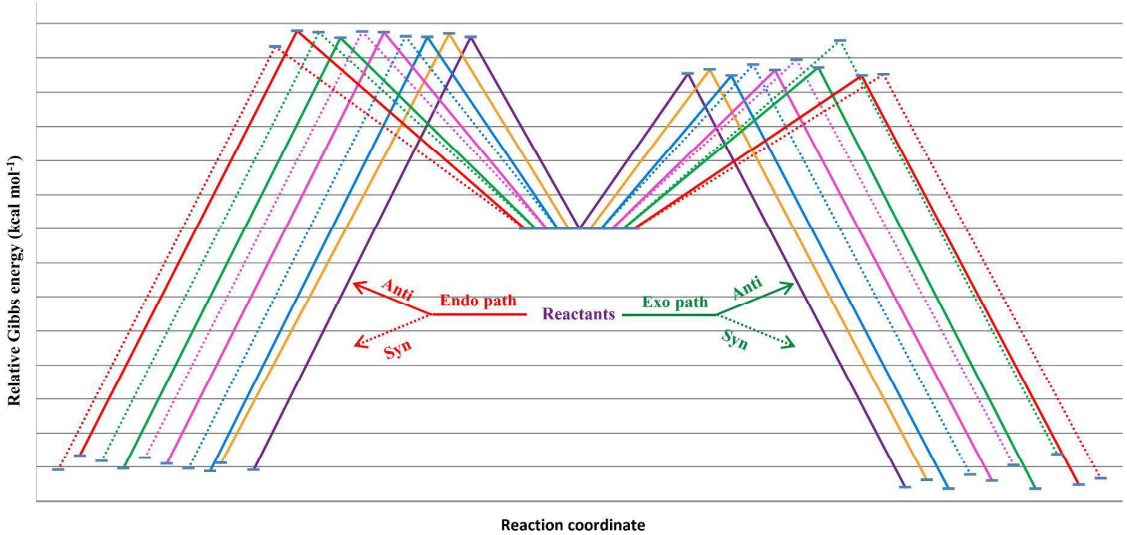

Figure 1. Potential energy diagrams for reactions of nitrile oxides (**1a, 1b**) and OBNDs (**2a-2d**): violet for **1a+2a**, orange for **1b+2a**, blue for **1a+2b**, pink for **1b+2b**, green for **1a+2c** and red for **1a+2d**. Solid and dotted lines indicate *anti* and *syn* regioisomeric channels, respectively.

For understanding the nature of the formed CA(s), at first, the structures of twenty TSs and related products as well as six reactants were fully optimized at B3LYP/6-31G(d) level of theory. IRC calculations were carried out for all studied reactions, and presented only for the reaction pathways leading to **3X (ba)** and **3N (ba)** in Figure S1. These calculations

show saddle points clearly, and demonstrate that the TSs connect to the associated minima. Total energies (in a.u.) for all species are shown in Table S2. Activation and reaction energies (kcal mol^{-1}) are summarized in Table 1. Moreover, single point calculations have been computed for B3LYP/6-31G(d) optimized reactants and TSs at the M05-2X(UF)/6-311++G(2d,2p) level of theory, as have been suggested by Simon and Goodman[18] for the calculation of the activation energies in organic reactions (Table S3). Hereafter, the energies at B3LYP/6-31G(d) level are reported, unless otherwise noted.

Table 1. Calculated activation and thermodynamic parameters, in kcal mol^{-1}, global electron density transfer (GEDT) values, in e, and synchronicity degrees[a] for the TSs

Structures	$\Delta G^{\ddagger}$[b]	$\Delta G^{\ddagger}_{M05}$[c]	$\Delta H^{\ddagger}$	$\Delta H^{\ddagger}_{M05}$[c]	ΔG_{rxn}[d]	$\Delta E^{\ddagger}$	$\Delta E^{\ddagger}_{d\ dipole}$[e]	$\Delta E^{\ddagger}_{d\ alkene}$[e]	$\Delta E^{\ddagger}_{d\ total}$[e]	$\Delta E^{\ddagger}_{i}$[e]	GEDT	$\Delta d_{TS/P}$
TSXA (aa)	22.7	23.5	10.5	11.3	-38.0	10.2	14.0	3.0	17.0	-6.8	0.016	0.11
TSNA (aa)	28.0	27.7	15.2	15.0	-35.4	15.1	15.8	6.6	22.4	-7.4	0.008	0.13
TSXA (ab)	23.3	23.7	10.5	10.8	-36.9	10.1	14.1	3.1	17.2	-7.1	0.000	0.10
TSNA (ab)	28.5	27.6	15.5	14.7	-34. 4	15. 4	15.7	6.6	22.3	-6.9	-0.007	0.12
TSXA (ba)	22.4	23.1	10.1	10.8	-38.2	9. 8	14.0	3.1	17.1	-7.3	0.010	0.14
TSNA (ba)	28.0	27.5	15.2	14.7	-35.6	15.0	15.8	6.6	22.4	-7.4	0.006	0.13
TSXS (ba)	24.0	24.7	11. 7	12.4	-36.1	11.3	14.6	3.7	18. 3	-6.9	0.008	0.06
TSNS (ba)	28.1	27.5	15.3	14.7	-35.2	15.2	15. 9	6.6	22. 5	-7.3	0.007	0.13
TSXA (bb)	23.2	23.5	10. 2	10.5	-37.0	9.8	14.1	3.1	17. 3	-7.5	-0.004	0.12
TSNA (bb)	28.7	27.7	15.5	14.5	-34.5	15.3	15. 7	6.6	22.3	-6.9	-0.011	0.12
TSXS (bb)	24.7	24.6	11.7	11.6	-34.7	11.4	14.9	3.7	18.6	-7.3	-0.009	0.04
TSNS (bb)	28.8	27.2	15.6	14.1	-33.6	15.5	16.0	6.8	22.8	-7.3	-0.010	0.11
TSXA (ca)	23.6	24.4	10.7	11.5	-38.2	10. 3	13.9	3.9	17.8	-7.6	0.001	0.20
TSNA (ca)	27.9	27.3	15.3	14.7	-35.2	15.2	15.8	6.7	22.5	-7.3	0.004	0.14
TSXS (ca)	27.5	27.6	14.4	14.4	-33.1	14.1	15.4	5.1	20.6	-6.5	-0.004	0.05
TSNS (ca)	28.7	27.6	15.7	14.7	-34. 1	15.6	16.2	6.9	23.1	-7.5	0.005	0.11
TSXA (da)	22.4	23.2	9.5	10.3	-37.6	9.2	14.0	3.2	17.2	-8.1	0.015	0.15
TSNA (da)	28.9	28.7	16.6	16.4	-33.3	16.4	15.8	7.0	22.8	-6.4	0.021	0.15
TSXS (da)	22.6	22.7	9.9	10.0	-36.7	9.5	14.7	3.8	18.5	-9.0	0.019	0.09
TSNS (da)	26.6	25.8	13.0	12.2	-35.4	12.7	15.9	7.2	23.1	-10.4	0.024	0.16

[a] $\Delta d_{TS/P} = |(C–C)_{TS}/(C–C)_{p} – (C–O)_{TS}/(C–O)_{p}|$
[b] $\Delta G^{\ddagger} = G(TS) - G(dipole) - G(dipolarophile)$
[c] The B3LYP Gibbs energy and enthalpy corrections have been added to the M05-2X(UF) single-point energies.[18]
[d] $\Delta G_{rxn} = G(product) - G(dipole) - G(dipolarophile)$
[e] $\Delta E^{\ddagger}_{d\ dipole}$, $\Delta E^{\ddagger}_{d\ alkene}$ and $\Delta E^{\ddagger}_{d\ total}$ are distortion energy of nitrile oxides, distortion energy of OBNDs and total distortion energy, respectively. $\Delta E^{\ddagger}_{i}$ indicates interaction energy between distorted fragments.

Calculated activation and thermodynamic parameters have been presented in Table 1 which indicates that all these 1,3-DC reactions are very exothermic, ranging from -33.1 to -38.2 kcal mol^{-1} and the *exo* products are thermodynamically more stable than *endo* stereoisomers. In addition, a comparison of the activation energies also indicates that in all cases the *exo* stereoisomers are the major products. The activation Gibbs energy differences between *exo* and *endo* forms in these 1,3-DCs are greater than 4.2 kcal mol^{-1}, demonstrate that the nitrile oxide dipoles prefer to approach the bicyclic framework from the *exo* face. Theoretical results for complete *exo*-stereoselectivity in these reactions are in agreement with experiment.[13]
Computed activation enthalpies associated with the most favorable reactive channel of these 1,3-DC reactions are in the range of 9.5-10.7 kcal mol^{-1}, in the gas phase, while the activation Gibbs energies are in the range of 22.4-23.6 kcal mol^{-1}. This behavior is mainly due to the bimolecular character of these cycloadditions, which present unfavorable activation entropy. The different substitution patterns render relatively small energy differences ($\Delta\Delta G^{\ddagger} \leq$ 1.2 kcal mol^{-1}), therefore, it can be concluded that the substituents effect at the carbon atom of dipoles and C1 atom of dipolarophiles is low on the energy barriers of these 1,3-DC reactions. However, these substituents cause to be produced different ratio of regioisomeric CAs. The relative amount of the two possible CAs is proportional to the relative energies of two the corresponding TSs. Based on the Gibbs energy activation of the TSs at 298 K, the Boltzmann distribution ratio has been calculated and reported in Table 2.

Table 2. Experimental and calculated regioisomeric ratios of CAs at 298 K

	3X (bb)/4X (bb)	3X (ba)/4X (ba)	3X (ca)/4X (ca)	3X (da)/4X (da)
Calculated (B3LYP)	93:7	94:6	100:0	58:42
Calculated (M05-2X)	86:14	94:6	100:0	30:70
Experimental	92:8	85:15	100:0	75:25

Calculated ratios are in harmony with the experimental results. B3LYP/6-31G(d) level of theory produces better results than M05-2X/6-311++G(2d,2P)//B3LYP/6-31G(d) level. The analysis of the regioselectivity of these 1,3-DC reactions measured as the difference of activation Gibbs energies ($\Delta\Delta G^{\ddagger}$) between the two regioisomeric pathways shows that while, only one regioisomer is formed with bulky $SiMe_3$ substituent at the C1 atom of **OBND** (**2c**), the mixture of regioisomeric CAs are obtained with other substituents (Table 2). For all reactions, formation of the *anti*-regioisomer CAs is preferred over the *syn*-regioisomers which is in agreement with the experimental outcome. Based on the energies, obtained from single point calculations at the M05-2X(UF)/6-311++G(2d,2p) level of theory for optimized reactants and TSs, the composition of regioisomers are not changed considerably, while for the regioisomeric mixture of **3X (da)** and **4X (da)** contradictory results are observed. At the B3LYP and M05-2X functionals, the activation energy of the *anti*-regioisomeric path is 0.2 and 0.5 kcal mol^{-1} lower and higher than *syn*-regioisomeric path, respectively. To analyze this contradiction, **TSXA (da)** and **TSXS (da)**

were fully optimized at the M05-2X(UF)/6-311++G(2d,2p) level, but the same results were obtained. For validation of the results obtained experimentally and in continuation of our recently studies on elucidation of regioselectivity by GIAO/^{13}C NMR calculations,[33] GIAO ^{13}C chemical shifts for **3X (da)** and **4X (da)** are computed by Sarotti and Pellegrinet method.[34] Experimental and unscaled GIAO ^{13}C chemical shift values of these two regioisomers calculated at mPW1PW91/6-31G(d)//B3LYP/6-31G(d) level of theory in the gas phase using multi-standard (MSTD) approach[34] are shown in Table 3. The experimental chemical shifts between the major and minor regioisomers are mostly different for C_1 atom ($|\Delta\delta|$=3.3 ppm) and C_4 atom ($|\Delta\delta|$=5.8 ppm). A comparison of the calculated chemical shifts of C_1 and C_4 atoms of the two regioisomers with their experimental data shows that **3X (da)** is the major regioisomer. Therefore, prediction of the regioselectivity of these 1,3-DC reactions by the B3LYP hybrid functional is more reliable than those obtained from M05-2X hybrid meta functional.

Table 3. Experimental and unscaled GIAO ^{13}C chemical shift values, in ppm, of **3X (da)** and **4X (da)** (atom numbering is according to Figure 2)

	C_{12}	C_{17}	C_5	C_6	C_8	C_9	C_7	C_{10}	C_1	C_2	C_4	C_3	C_{13}	C_{18}
3X (da) (calculated)	206.5	152.6	144.6	142.3	128.4	128.3	124.1	120.3	**96.6**	90.9	**80.0**	63.7	29.7	13.4
3X (da) (Exp.)	204.8	152.6	143.8	139.9	128.4	127.8	121.1	119.8	**96.9**	88.1	**79.3**	63.1	28.7	12.0
4X (da) (calculated)	207.9	151.2	145.8	142.3	128.4	128.5	122.0	121.4	**94.6**	88.6	**85.1**	66.0	29.0	14.7
4X (da) (Exp.)	205.3	151.1	143.4	140.8	128.3	128.0	121.1	119.5	**93.6**	87.9	**85.1**	63.8	28.5	13.0

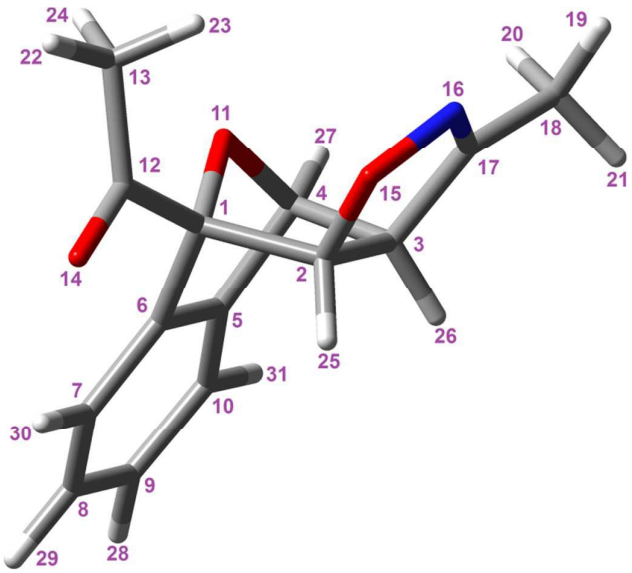

Figure 2. Optimized structure of **3X (da)** with atom numbering

The geometries of the TSs, the lengths of the C-C and C-O forming bonds and their Wiberg bond order (BO) values at the TSs are shown in Figure 3. Analysis of the lengths of the two forming bonds at the TSs shows that they are not formed to the same extent. Although in all products, C-O bond length is shorter than C-C one (1.44 A° versus 1.51 A°), their values are inverse at the TSs. This suggests that the C-C bond formations at the TSs are more advanced than the C-O bond formations. As a measure of asynchronicity, the parameter $\Delta d_{TS/P}$, defined as the difference between the ratios of the forming bond lengths at the TS and the corresponding bond lengths in the product, was proposed.[35] Their values range from 0.10 to 0.20 for *exo* and *anti*-channels (Table 1) suggest that the reactions are low asynchronous. An observable general trend is that the *exo/anti* TSs are consistently more asynchronous than the *exo/syn* TSs with $\Delta d_{TS/P}$ values range from 0.04 to 0.09 in the gas phase, indicating the latters are almost synchronous. Note that in the *exo* TSs, the C-C and C-O forming bonds are longer than the *endo* ones, indicating earlier TSs. The extent of the bond formation can also be provided by the BO analysis[36] at the TS. Hence, the BO values for all forming bonds are calculated and given in Figure 3. These BO values are in the range of 0.24 to 0.28 for C-C bonds and 0.18 to 0.21 for C-O bonds. These BOs clearly indicate that the bond-formation of C-C are slightly more advanced than C-O bonds.

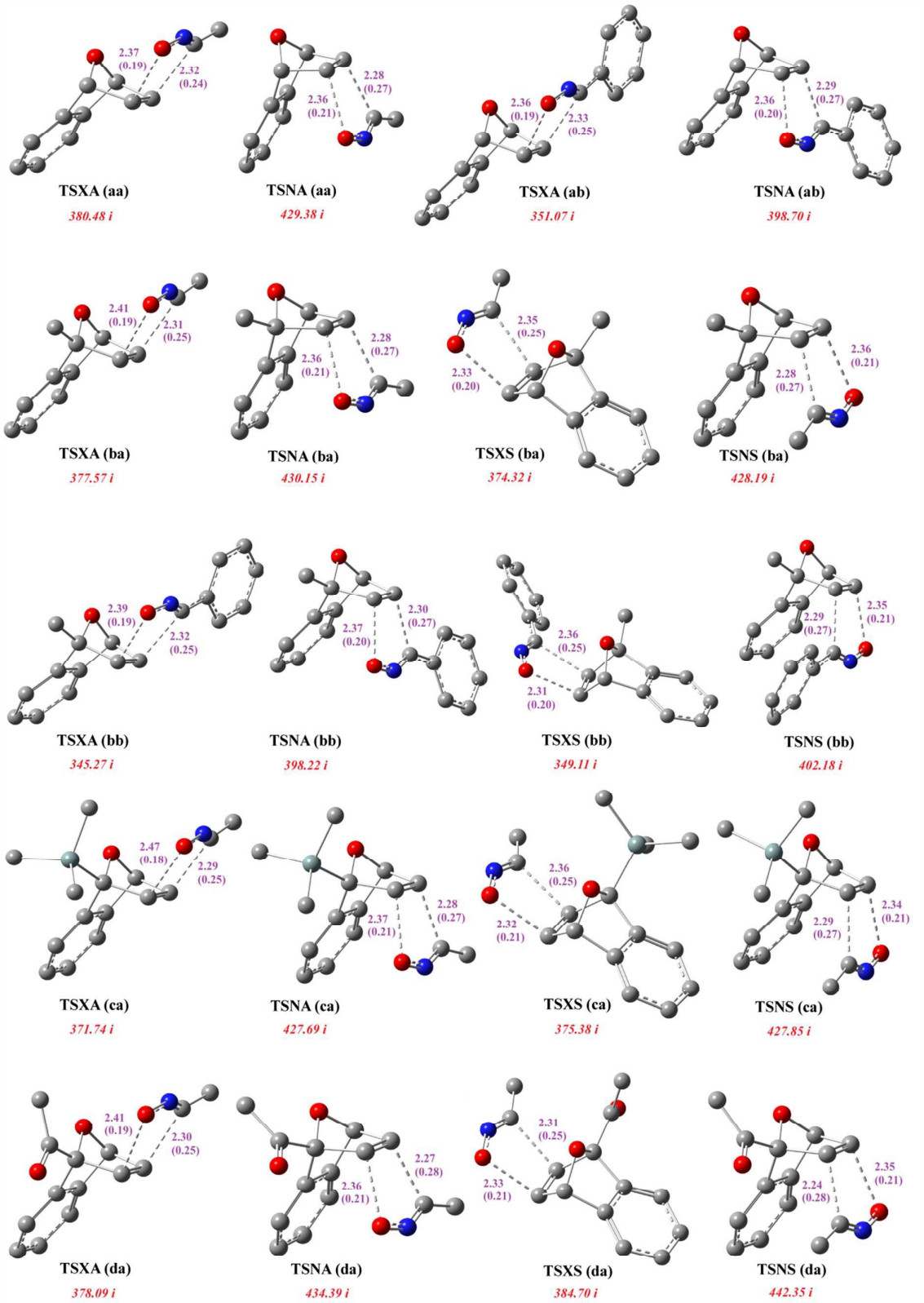

Figure 3. Geometries of TSs of the 1,3-DC reactions between nitrile oxides (**1a, 1b**) and OBNDs (**2a-2d**). The imaginary frequencies are given in cm^{-1} and bond distances in A° units. BO values are given in parenthesis.

3.3. The origin of regio- and stereoselectivity

The distortion/interaction model which is an approach to dissect the activation barriers into distortion energy and interaction energy has been used recently in explaining of the stereoselectivity of norbornene in hetero Diels–Alder[37] and Azide Cycloaddition[38] reactions. This model is also used in order to gain a deeper insight into *anti* and *exo* selectivity of C_1-substituted OBNDs with nitrile oxides. The distortion of OBNDs and 1,3-dipoles in the transition structures has been taken into account by comparing their structure prior to the cycloaddition to the one in the TSs. The computed activation barriers ($\Delta G^{\ddagger}$, $\Delta H^{\ddagger}$, $\Delta E^{\ddagger}$), distortion ($\Delta E_d^{\ddagger}$) and interaction ($\Delta E_i^{\ddagger}$) energies in each transition structure are reported in Table 1. The activation energies ($\Delta E^{\ddagger}$), interaction and distortion energies are in a range of 9.2-16.4, 6.4–10.4 and 17.0-23.1, in kcal mol^{-1}, respectively. This shows that the activation energy is governed mainly by the distortion energy. Figure 4 shows a plot of $\Delta E^{\ddagger}$ versus $\Delta E_d^{\ddagger}$ for the studied reactions. There is a fair linear correlation ($r^2 = 0.89$) between the reactant distortion energies and activation energies, because of the existence of two outliers, **TSXS (da)** and **TSNS (da)**. An excellent linear correlation is observed ($r^2 = 0.98$) when the mentioned two outliers are omitted. The activation barriers for these cases deviate because their interaction energy in their TSs is greater than the other TSs (Table 1).

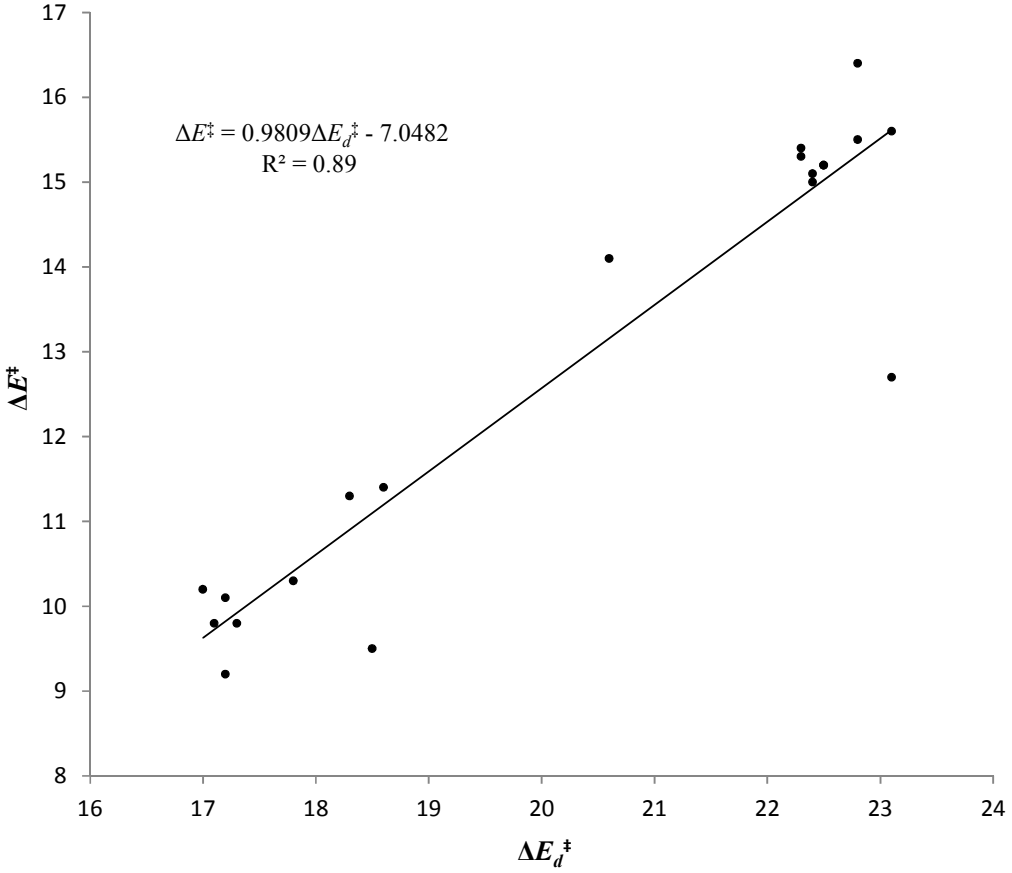

Figure 4. Theoretical correlation of the activation energies and distortion energies, in kcal mol^{-1}, at the B3LYP/6-31G(d) level

The range of OBND distortion energies (3−7.2 kcal mol^{-1}) is larger than that of distortion energies of nitrile oxides (13.9−16.2 kcal mol^{-1}), although the latter are generally larger than the former. It was previously shown with 1,3-DC of acetylene and ethylene with many dipoles, the distortion of the 1,3-dipole is about 80% of the distortion energy.[39] In the nitrile oxide cycloaddition studied here, dipole distortion energies comprise 75-82% of the total distortion energies in the *exo* transition structures. In the case of *endo*, dipole distortion energy makes up 70% of the total distortion energy. Nitrile oxides in the *exo* and *endo* transition structures have ∠CNO = 145° and 143°, respectively, hence distortion energies of dipoles are almost similar in all reactions.

On the other hand, the distortion of dipolarophiles comprises ~20% of the total distortion energy in the *exo* transition structures while it makes up ~30% of the total distortion energy in the *endo* ones. This portion of the distortion energy is the energy required to distort OBNDs from their equilibrium structures, indicating that in the *endo* transition structures, dipolarophiles are 1.5 fold more distorted than the *exo* transition structures.

For understanding the origin of OBNDs distortion energy differences in *exo* and *endo* TSs, and in the light of the large distortion which is mostly associated with C–H bonds bending out of plane in OBNDs, six dihedral angles that are changed more along the reaction have been monitored. θ_1 ($C_1C_2C_3H_{26}$), θ_2 ($C_4C_3C_2H_{25}$), θ_3 ($O_{11}C_1C_2H_{25}$), θ_4 ($O_{11}C_4C_3H_{26}$), θ_5

($H_{25}C_2C_1R$) and θ_6 ($H_{26}C_3C_4H_{27}$) (for atom numbering see Figure 2). These dihedral angle values in the optimized reactants and TSs are shown in Table S4. θ_1 and θ_2 values from reactants to the TSs change in a range of 11.2-22.3°; however, these changes are almost the same for *exo* and *endo* pathways for each reaction (0-3.8°). On the other hand, not only changes of θ_3, θ_4, θ_5 and θ_6 are large (12.2-32.8° for θ_3 and θ_4 as well as 11.8-31.8° for θ_5 and θ_6), but are also different for two stereoisomers (8.5-13.2° for θ_3 and θ_4 as well as 6.8-11.6° for θ_5 and θ_6). As shown in Table S4, these dihedral angles in *endo* TSs change more than *exo* ones. There is not any correlation between $\Delta E_{\text{d alkene}}$ and the sum of the θ_1 and θ_2 dihedral angles, but a good linear correlation is observed (r^2 = 0.97) for $\Delta E_{\text{d alkene}}$ and $\sum_{i=3}^{6} \theta i$ (Figure 5). Moreover, the *exo* stereoselectivity seen in these reactions also results from different torsional effects in *exo* and *endo* TSs. Figure 6 shows Newman projections along the C_1-C_2 and C_3-C_4 bonds in the **TSXA (ba)** and **TSNA (ba)**. While the former is almost in the staggered conformation about these bonds, the latter shows a nearly perfect eclipsing.

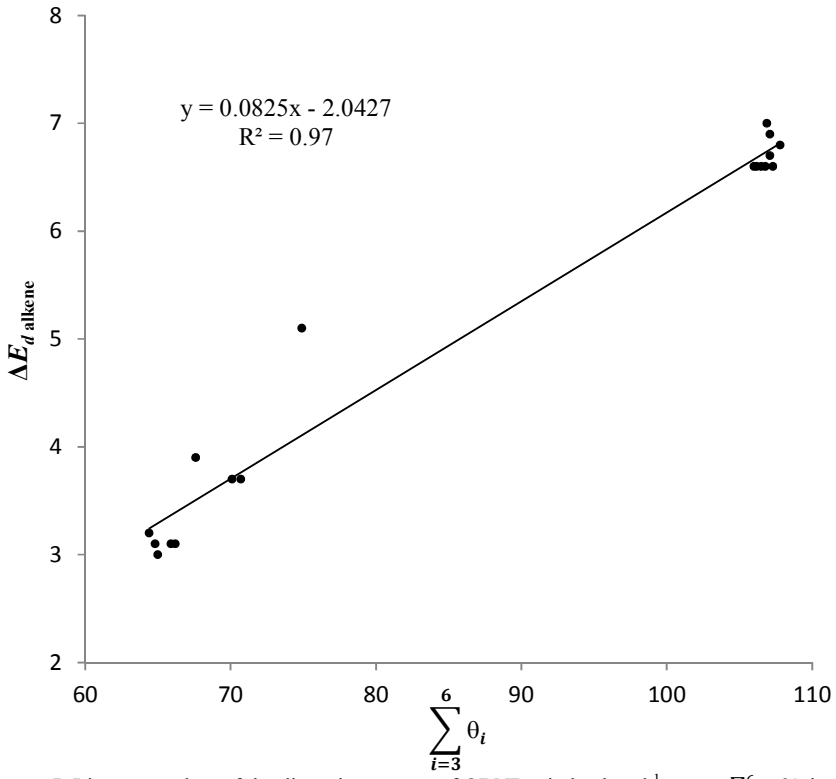

Figure 5. Linear correlate of the distortion energy of OBNDs, in kcal mol^{-1} versus $\sum_{i=3}^{6} \theta i$, in deg

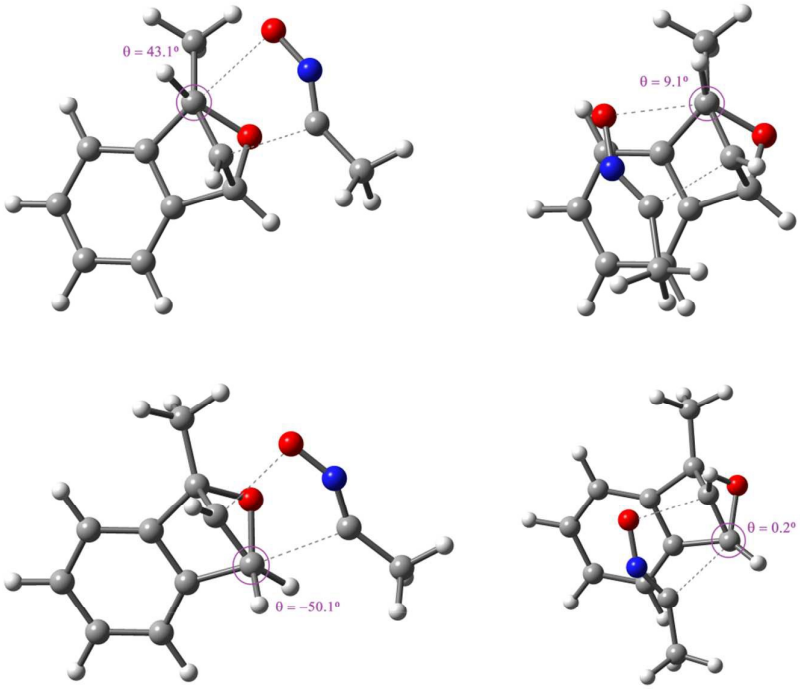

Figure 6. Newman projections for **TSXA (ba)** (left) and **TSNA (ba)** (right).

Distortion/interaction model is also able to explain regioselectivity in these reactions. The lower distortion energy of *anti* regioisomers than *syn* regioisomers (1.2-2.8 kcal mol^{-1}), together with their higher stabilizing interactions (0.2-1.1 kcal mol^{-1}), except for **TSXA (da)** (Table 1) make the *anti* regioisomers more stable and appears to be the major regioisomer. Distortion energy differences of two regioisomeric channels are equal in the reaction of **2b** and **2d** with nitrile oxides; however, Gibbs energy differences are different. Stabilizing interactions energy at **TSXS (da)** is 0.9 kcal mol^{-1} more than **TSXA (da)**, hence their Gibbs energy difference is only reduced to 0.2 kcal mol^{-1}.

4. Conclusion

The 1,3-DC reactions of some C_1-substituted OBNDs (**2a-2d**) with nitrile oxides (**1a-1b**) has been investigated theoretically for each plausible type of approach of 1,3-dipoles to OBNDs. It is found that *exo* CAs are preferred because of the lower distortion of strained dipolarophiles and the lower torsional effects, present in the related TSs. Among the *exo* TSs, *anti* regioisomers are more stable than *syn* ones because of the lower distortion and more favorable interactions. The calculated population of products, based on the Gibbs energy of TSs, reflects the experimental findings. GIAO/^{13}C NMR calculations were used for elucidation of regioselectivity in these reactions.
Our calculations show these cycloadditions take place through a low asynchronous one-step mechanism with a none polar character and classified as (*pseudodiradical*) *pr-type* 1,3-DC reactions. In most cases, the B3LYP and M05-2X results were consistent with experiments. However, in a few cases, under the assumption of the conventional transition state theory, the B3LYP method seemed to give more reasonable results.

Acknowledgements

The authors are thankful to the Research Council of Ferdowsi University of Mashhad, Iran (Grant no. 3/29786) for financial support.

Notes and references

Department of Chemistry, Faculty of Sciences, Ferdowsi University of Mashhad, Mashhad 91775-1436, Iran.
Corresponding author: Javad Tajabadi (e-mail: javad.tajabadi@stu.um.ac.ir).
Tel/Fax: +985138795457

Electronic Supplementary Information (ESI) available: Calculated geometries and energies. See DOI: 10.1039/b000000x/

1 D. Giomi, F.M. Cordero and F. Machetti, *Comprehensive Heterocyclic Chemistry III*, 2008, **4**, 365.
2 (a) A. B. V. K. Kumar, A. U. R. Sankar and S. H. Kim, *Journal of Heterocyclic Chemistry,* 2014, **51**, E146; (b) Basappa, M. P. Sadashiva, K. Mantelingu, S. N. Swamy and K. S. Rangappa, *Bioorg. Med. Chem.*, 2003, **11**, 4539.

3 E. Ghidini, A.M. Capelli, C. Carnini, V. Cenacchi, G. Marchini, A. Virdis, A. Italia and F. Facchinetti, *Steroids*, 2015, **95**, 88.

4 (a) M. P. Curtis, N. Chubb, E. Ellsworth, R. Goodwin, S. Holzmer, J. Koch, T. McTier, S. Menon, K. Mills, A. Pullins, T. Stuk and E. Zinser, *Bioorganic & Medicinal Chemistry Letters*, 2014, **24**, 5011; (b) M. Gassel, C. Wolf, S. Noack, H. Williams and T. Ilg, *Insect Biochemistry and Molecular Biology*, 2014, **45**, 111; (c) I. T. Hwang, H. R. Kim, D. J. Jeon, K. S. Hong, J. H. Song and K. Y. Cho, *J. Agric. Food Chem.*, 2005, **53**, 8639; (d) C. Zhao and J. E. Casida, *J. Agric. Food Chem.*, 2014, **62**, 1019.

5 (a) K. Kaur, V. Kumar, A. K. Sharma and G. K. Gupta, *European Journal of Medicinal Chemistry*, 2014, **77**, 121; (b) Basappa, M. P. Sadashiva, S. N. Swamy, F. Li, K. A. Manu, M. Sengottuvelan, D. S. Prasanna, N. C. Anilkumar, G. Sethi, K. Sugahara and K. S. Rangappa, *BMC Chem. Biol.*, 2012, **12**, 5; (c) J. Khazir, P. P. Singh, D. M. Reddy, I. Hyder, S. Shafi, S. D. Sawant, G. Chashoo, A. Mahajan, M. S. Alam, A. K. Saxena, S. Arvinda, B. D. Gupta and H. M. S. Kumar, *European Journal of Medicinal Chemistry*, 2013, **63**, 279.

6 C. Kouklovsky and G. Vincent, *Reference Module in Chemistry, Molecular Sciences and Chemical Engineering*, from *Comprehensive Organic Synthesis II (Second Edition)*, 2014, **8**, 493.

7 (a) V. Jager and P. A. Colinas, In *Synthetic Applications of 1.3-Dipolar Cycloaddition Chemistry Toward Heterocycles and Natural Products*, A. Padwa and W.H. Pearson, Eds. Wiley: New York, ISBN 0-471-38726-6, 2003, 361; (b) N. Dorostkar-Ahmadi, M. Bakavoli, F. Moeinpour and A. Davoodni, *Spectrochimica Acta Part A: Molecular and Biomolecular Spectroscopy*, 2011, **79**, 1375; (c) M. Bakavoli, F. Moeinpour, A. Sardashti-Birjandi and A. Davoodnia, *J. Heterocyclic Chem.*, 2013, **50**, 188.

8 (a) D. K. Rayabarapu and C. H. Cheng, *Acc. Chem.Res.*, 2007, **40**, 971; (b) M. Lautens, K. Fagnou and S. Heibert, *Acc. Chem.Res.*, 2003, **36**, 48; (c) W. Tam and N. Cockburn, *Synlett*, 2010, **8**, 1170; (d) J. Hu, Q. Yang, J. Xu, C. Huang, B. Fan, J. Wang, C. Lin, Z. Bian and A. S. C. Chan, *Org. Biomol. Chem.*, 2013, **11**, 814.

9 (a) N. B. Darvatkar, K. S. Wankhede, S. V. Bhilare, A. R. Deorukhkar, D. G. Raut, V. V. Vaidya, G. K. Trivedi and M. M. Salunkhe, *J. Heterocyclic Chem.*, 2010, **47**, 1004; (b) R. Huisgen, P. H. J. Oohrns, M. Mingin and N. L. Allinger, *J. Arner. Chern. Soc.*, 1980, **102**, 3951; (c) G. Singh, M. Elango, V. Subramanian and M. P. S. Ishar, *Heterocycles*, 2006, **68**, 1409; (d) S. V. Chapyshev and V. M. Anisimov, *Chemistry of Heterocyclic Compounds*, 1997, **33**, 1315; (e) M. Gucma, W. M. Golebiewski and M. Krawczyk, *J. Braz. Chem. Soc.*, 2013, **24**, 805.

10 (a) L. Jaroskkova and L. Fisera, *Collect. Czech. Chem. Commun.*, 1993, **58**, 588; (b) L. Fisera and D. Pavlovic, *Collect. Czech. Chern.Commun.*, 1984, **49**, 1990; (c) T. Sasaki, S. Eguchi, M. Yamaguchi, and T. Esaki, *J. Org. Chem.*, 1981, **46**, 1800; (d) T. Sasaki, K. Kanernatsu, K. Kayakawa and M. Vchide, *J. Chem. Soc., Perkin Trans. I*, 1972, 2750; (e) E. Jedlovska and L. Fisera, *Chem. Papers*, 1991, **45**, 419; (f) E. Jedlovska and L. Fisera, *Chem. Papers*, 1992, **46**, 238; (g) J. Plumet, G. Escobar, C. Manzano, O. Arjona, P. A. Carrupt and P. Vogel, *Heterocycles*, 1986, **24**, 1535; (h) V. Rajkumar, N. A. Aslam, C. Reddy and S. A. Babu, *Synlett*, 2012, **23**, 549.

11 (a) O. Arjona, A. Dios, R. F. Pradilla, A. Mallo and J. Plumet, *Tetrahedron*, 1990, **46**, 8179; (b) O. Arjona, C. Dominguez, R. F. Pradilla, A. Mallo, C. Manzano and J. Plumet, *J. Org. Chem.*, 1989, **54**, 5883; (c) P. Mayo, T. Hecnar and W. Tam, *Tetrahedron*, 2001, **57**, 5931; (d) I. N. N. Namboothiri, N. Rastogi, B. Ganguly, S. M. Mobin and M. Cojocaru, *Tetrahedron*, 2004, **60**, 1453.

12 (a) H. Taniguchi, T. Ikeda, Y. Yoshida and E. Imoto, *Chemistry Letters*, 1976, **5**, 1139; (b) H. Taniguchi, T. Ikeda, Y. Yoshida and E. Imoto, *Bull. Chem. Soc. Jpn.*, 1977, **50**, 2694; (c) T. Hisano, K. Harano, T. Matsuoka, T. Suzuki and Y. Murayama, *Chem. Pharm. Bull.*, 1990, **38**, 605; (d) C. Micheli, R. Gandolfi and R. Oberti, *J. Org. Chem.*, 1980, **45**, 1209; (e) K. Tanaka, H. Masuda and K. Mitsuhashi, *Bull. Chem. Soc. Jpn.*, 1986, **59**, 3901.

13 (a) J. R. Nagireddy, E. Carlson and W. Tam, *Can. J. Chem.*, 2014, **92**, 1053; (b) J. R. Nagireddy, E. Carlson and W. Tam, *Can. J. Chem.*, 2014, **92**, 635.

14 (a) J. Tajabadi, M. Bakavoli, M. Gholizadeh, H. Eshghi and A. Khojastehnezhad, *Progress in Reaction Kinetics and Mechanism*, 2014, **39**, 233; (b) M. Rahimizadeh, H. Eshghi, A. Khojastehnezhad, F. Moeinpour, M. Bakavoli and J. Tajabadi, *J. Fluorine. Chem.*, 2014, **162**, 60.

15 Gaussian 09, M. J. Frisch, G. W. Trucks, H. B. Schlegel, G. E. Scuseria, M. A. Robb, J. R. Cheeseman, G. Scalmani, V. Barone, B. Mennucci, G. A. Petersson, H. Nakatsuji, M. Caricato, X. Li, H. P. Hratchian, A. F. Izmaylov, J. Bloino, G. Zheng, J. L. Sonnenberg, M. Hada, M. Ehara, K. Toyota, R. Fukuda, J. Hasegawa, M. Ishida, T. Nakajima, Y. Honda, O. Kitao, H. Nakai, T. Vreven, J. A. Montgomery, Jr., J. E. Peralta, F. Ogliaro, M. Bearpark, J. J. Heyd, E. Brothers, K. N. Kudin, V. N. Staroverov, R. Kobayashi, J. Normand, K. Raghavachari, A. Rendell, J. C. Burant, S. S. Iyengar, J. Tomasi, M. Cossi, N. Rega, J. M. Millam, M. Klene, J. E. Knox, J. B. Cross, V. Bakken, C. Adamo, J. Jaramillo, R. Gomperts, R. E. Stratmann, O. Yazyev, A. J. Austin, R. Cammi, C. Pomelli, J. W. Ochterski, R. L. Martin, K. Morokuma, V. G. Zakrzewski, G. A. Voth, P. Salvador, J. J. Dannenberg, S. Dapprich, A. D. Daniels, O. Farkas, J. B. Foresman, J. V. Ortiz, J. Cioslowski, and D. J. Fox, Gaussian, Inc., Wallingford CT, 2009.

16 (a) A. D. Becke, *J. Chem. Phys.*, 1993, **98**, 5648; (b) C. Lee, W. Yang and R.G. Parr, *Phys. Rev. B*, 1988, **37**, 785; (c) W. J. Hehre, L. Radom, P. V. R. Schleyer and J. A. Pople, *Ab Initio Molecular Orbital Theory*, Wiley: New York, NY, 1986.

17 G. O. Jones, D. H. Ess and K. N. Houk, *Helv. Chim. Acta*, 2005, **88**, 1702.

18 L. Simon and J. M. Goodman, *Org. Biomol. Chem.*, 2011, **9**, 689.

19 GaussView, Version 5, R. Dennington, T. Keith and J. Millam, *Semichem Inc*., Shawnee Mission, KS, 2009.

20 C. Gonzalez and H. B. Schlegel, *J. Phys. Chem*., 1990, **94**, 5523; (b) C. Gonzalez and H. B. Schlegel, *J. Phys. Chem*., 1991, **95**, 5853.

21 (a) D. H. Ess and K. N. Houk, *J. Am. Chem. Soc.*, 2007, **129**, 10646; (b) D. H. Ess and K. N. Houk, *J. Am. Chem. Soc.*, 2008, **130**, 10187; (c) T. Ziegler and A. Rauk, *Theor. Chim. Acta*, 1977, **46**, 1; (d) T. Ziegler and A. Rauk, *Inorg.Chem.*, 1979, **18**,1755; (e) F. M. Bickelhaupt, T. Ziegler and P. V. R. Schleyer, *Organometallics*, 1995, **14**, 2288.

22 (a) A. E. Reed, R. B. Weinstock and F. Weinhold, *J. Chem. Phys.*, 1985, **83**, 735; (b) A. E. Reed, L. A. Curtiss and F. Weinhold, *Chem. Rev.*, 1988, **88**, 899.

23 (a) P. Geerlings, F. De Proft and W. Langenaeker*, Chem. Rev.*, 2003, **103**, 1793; (b) D. H. Ess, G. O. Jones and K. N. Houk, *Adv. Synth. Catal.*, 2006, **348**, 2337.

24 R.G. Parr, L. Von Szentpaly and S. Liu, *J. Am. Chem. Soc.*, 1999, **121**, 1922.

25 R.G. Parr and R.G. Pearson, *J. Am. Chem. Soc*., 1983, **105**, 7512; (b) R.G. Parr and W. Yang, In: *Density functional theory of atoms and molecules*, 1989, Oxford University, New York, NY.

26 L.R. Domingo, E. Chamorro and P. Perez, *J. Org. Chem*., 2008, **73**, 4615; (b) L.R. Domingo and P. Perez, *Org. Biomol.Chem*., 2011, **9**, 7168.

27 M. J. Aurell, L. R. Domingo, P. Perez and R. Contreras, *Tetrahedron*, 2004, **60**, 11503.

28 L. R. Domingo, M. J. Aurell, P. Perez, and R. Contreras, *Tetrahedron*, 2002, **58**, 4417.

29 P. Jaramillo, L. R. Domingo, E. Chamorro and P. Perez, *J. Mol. Struct. (Theochem)*, 2008, **865**, 68.

30 P. Perez, L. R. Domingo, M. J. Aurell and R. Contreras, *Tetrahedron*, 2003, **59**, 3117.

31 L. R. Domingo and S. R. Emamian, *Tetrahedron*, 2014, **70**, 1267.

32 L. R. Domingo, P. Perez, and J. A. Saez, *RSC Advances*, 2013, **3**, 1486.

33 M. Bakavoli, H. Eshghi, A. Shiri, T. Afrough, and J. Tajabadi, *Tetrahedron*, 2013, **69**, 8470.

34 A. M. Sarotti and S. C. Pellegrinet, *J. Org. Chem.*, 2009, **74**, 7254.

35 A. Contini, S. Leone, S. Menichetti, C. Viglianisi and P. Trimarco, *J. Org. Chem.*, 2006, **71**, 5507.

36 K. B. Wiberg, *Tetrahedron*, 1968, **24**, 1083.

37 S. A. Cinar, S. Ercan, S. E. Gunal, I. Dogan and V. Aviyente, *Org. Biomol. Chem.*, 2014, **12**, 8079.

38 S. A. Lopez and K. N. Houk, *J. Org. Chem.*, 2013, **78**, 1778.

39 C. Gordon, J. L. Mackey, J. C. Jewett, E. M. Sletter, K. N. Houk and C. R. Bertozzi, *J. Am. Chem. Soc.*, 2012, **134**, 9199.